China Ocean Eng., 2017, Vol. 31, No. 1, P. 114–122
DOI: 10.1007/s13344-017-0014-5, ISSN 0890-5487
http://www.chinaoceanengin.cn/ E-mail: coe@nhri.cn

Study on Pure IL VIV of A Free Spanning Pipeline Under General Boundary Conditions

XU Wan-hai[a, b], XU Jing-yu[c], WU Ying-xiang[c, *], JI Chun-ning[a]

[a]State Key Laboratory of Hydraulic Engineering Simulation and Safety, Tianjin University, Tianjin 300072, China

[b]Collaborative Innovation Centre for Advanced Ship and Deep-Sea Exploration, Shanghai 200240, China

[c]Institute of Mechanics, Chinese Academy of Sciences, Beijing 100190, China

Received January 14, 2015; revised October 28, 2015; accepted January 12, 2016

Abstract

Pipeline spans may occur due to natural seabed irregularities or local scour of bed sediment. The pure in-line (IL) vortex-induced vibrations (VIV) analysis of the free spans is an important subject for design of pipeline in uneven seabed. The main objective of this paper is to analyze the characteristics of pure IL VIV of a free spanning pipeline under general boundary conditions. An IL wake oscillator model which can describe the coupling of pipeline structure and fluctuating drag is introduced and employed. The coupled partial differential equations of structure and wake are transformed into a set of ordinary differential equations using two-mode Galerkin method. Some case studies are presented and thoroughly discussed in order to investigate the effects of internal fluid, axial force and boundary conditions on the pure IL VIV.

Key words: free spanning pipeline, vortex-induced vibrations, boundary conditions, internal fluid

Citation: Xu, W. H., Xu, J. Y., Wu, Y. X., Ji, C. N., 2017. Study on pure IL VIV of a free spanning pipeline under general boundary conditions. China Ocean Eng., 31(1): 114–122, doi: 10.1007/s13344-017-0014-5

1 Introduction

Pipelines are key equipments for transportation of oil and gas from offshore oil wells to an onshore location in offshore petroleum fields. The pipelines usually encounter free spans owing to uneven seabed. When ocean flow passes these free spans, vortex-induced-vibrations (VIV) may occur in the in-line (IL) and cross-flow (CF) directions due to the periodically shed vortices in the near-wake (see Fig. 1). VIV is an important cause of fatigue damage of pipelines at the free spanning sections. Over decades, many researchers have focused on this complex but interesting phenomenon, especially the links between structure responses and near-wake patterns, and several comprehensive reviews can be found in Blevins (1990), Sarpkaya (2004), Gabbai and Benaroya (2005) and Williamson and Govardhan (2008).

The VIV response of free spanning pipelines is affected by boundary conditions, axial force, internal flow, and etc. Yeganeh Bakhtiyary et al. (2007) investigated the effect of soil boundary conditions, together with axial force on natural frequency of offshore pipelines. Ai et al. (2009) developed a time domain method for nonlinear pipe-seabed interaction analysis of free spanning pipelines under CF VIV conditions. Yaghoobi et al. (2012) investigated the influence of soil characteristics on the natural frequency of free spanning pipelines under several boundary conditions. Furnes and Berntsen (2003) proposed a prediction model, and discussed some dynamical features, mainly focused on the coupling between CF and IL VIV of tensioned free spanning pipelines subjected to current forces. Choi (2001) established a rigorous procedure on the free span analysis of offshore pipelines, and derived the closed form solutions of the beam-column equation for various possible boundary conditions. Fyrileiv (2010) showed the influence of internal pressure on free spanning pipelines. Lou et al. (2005) investigated the effects of internal fluid on the CF VIV of free spanning pipelines, and found the resonance frequency shifting to a lower frequency value. Koushan (2009) demonstrated the influence from temperature variation and soil boundary conditions on CF VIV in detail, and developed an improved strategy for non-linear analysis of free span pipeline. Huang et al. (2010) carried out a study on the fluid-structure interaction in pipeline conveying fluid, and obtained the natural frequency equation under different bound-

Foundation item: This research was financially supported by the National Natural Science Foundation of China (Grant Nos. 51479135, 51525803 and 51679167), the Science Fund for Creative Research Groups of the National Natural Science Foundation of China (Grant No. 51321065), and the Major State Basic Research Development Program of China (973 Program, Grant No. 2014CB046801).

*Corresponding author. E-mail: yxwu@imech.ac.cn

ary conditions by employing the eliminated element-Galerkin method. Dai et al. (2013) investigated the CF VIV of a hinged-hinged pipe conveying fluid by considering the internal fluid velocities ranging from the subcritical to the supercritical regions. Vedeld et al. (2013) introduced a semi-analytical model for the dynamics analysis of pipelines with free spans, and found that Euler-Bernoulli beam theory is sufficient with regard to pipeline free span modeling.

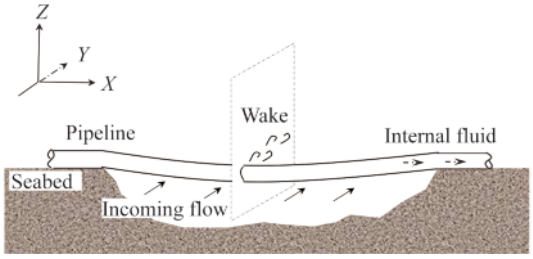

Fig. 1. A free spanning pipeline conveying fluid.

Although, the CF VIV of a free spanning pipeline has been thoroughly investigated, few studies have been done on the pure IL VIV case. Because the pure IL VIV in many cases will contribute significantly to fatigue damage for free spanning pipelines, more and more attention has been paid to this subject recently. Currie and Turnbull (1987) developed a wake oscillator model for pure IL VIV prediction, and they thought that the cylinder oscillations in the second instability region were a simple harmonic of the velocity driven transverse cylinder oscillations, while those in the first instability region might be amplitude driven. Larsen et al. (2007) presented an analysis model for pure IL VIV of free spanning pipelines, and illustrated some important features of pure IL VIV response. Lee et al. (2009) experimentally and computationally investigated the effects of the pipe stiffness on its first mode IL VIV in the reduced velocity ranging from approximately 1.0 to 4.0. Xu et al. (2012) proposed an acceleration coupling wake oscillator model for pure IL VIV of free spanning pipelines, and the comparisons between model results and experimental data showed quite good agreement.

It should be pointed out that, although some of the above studies have been focused on the effect of internal fluid, axial force and boundary conditions on the VIV of free spanning pipelines, they were mainly limited to VIV in the CF direction. To the best knowledge of the authors, in existing literatures, little research has been done about these effects on pure IL VIV of a free spanning pipeline. The purpose of this paper is to investigate the influences of internal fluid, axial force and boundary conditions on pure IL VIV. The results may be useful for researchers attempting to obtain more understanding on the behaviors of pure IL VIV.

The arrangement of the rest of this paper is as follows. In Section 2, we present an IL wake oscillator model to describe the coupling of a free spanning pipeline structure and fluctuating drag force. In Section 3, the Galerkin method is utilized to truncate the nonlinear partial differential equations into a set of ordinary differential equations. We validate the applicability and usefulness of the IL wake oscillator model to predict pure IL VIV of free spanning pipelines in Section 4. The influences of internal fluid, axial force and boundary conditions on pure IL VIV are discussed in details in Section 5. Finally, some conclusions are drawn in Section 6.

2 A wake oscillator model for pure IL VIV

2.1 Prediction model description

Let us consider a free spanning pipeline that conveys internal fluid as shown in Fig. 2, supposing that the internal fluid is inviscid and incompressible, and the deformation of free spans is small. The structural governing equation of the IL motion is based on the Euler-Bernoulli beam theory, and can be written as:

$$M\frac{\partial^2 Y}{\partial t^2}+C_{\mathrm{D}}\rho D U\frac{\partial Y}{\partial t}+2M_{\mathrm{f}}V_{\mathrm{f}}\frac{\partial^2 Y}{\partial X\,\partial t}+EI\frac{\partial^4 Y}{\partial X^4}+\left(M_{\mathrm{f}}V_{\mathrm{f}}^2-T\right)\frac{\partial^2 Y}{\partial X^2}=\frac{1}{2}\rho D U^2 C_{\mathrm{D}}', \tag{1}$$

where M is the total mass per unit length, including added mass M_{a}, structural mass M_{s} and internal fluid mass M_{f}, Y is the pipeline displacement in the IL direction, t is the time, and X is the coordinate along the pipeline, respectively. C_{D} is the mean drag coefficient, ρ is the ocean flow density, D is the uniform pipeline diameter, V_{f} is the constant internal fluid velocity, EI is the bending stiffness of the pipeline, T is the axial force (it is positive when the pipeline is stretched, and negative when the pipeline is compressed), U is the in-

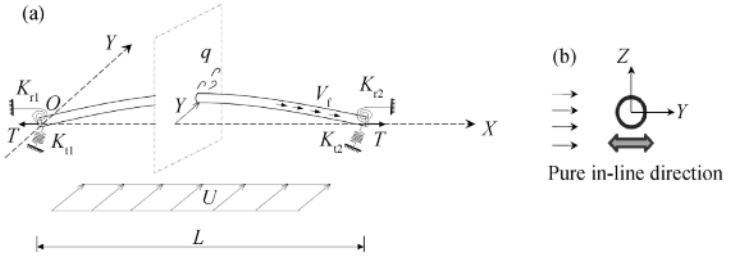

Fig. 2. Pipeline model with elastic restraints subject to a constant axial froce: (a) Definition of parameters and (b) Definition of IL direction.

coming ocean flow velocity, and C'_{D} is the fluctuating drag coefficient.

Generally, the free spans of the pipelines were modeled under idealized end boundary conditions (pinned or fixed) (Lou et al., 2005; Xu et al., 2012). In order to provide reasonable boundary conditions from the pipe laying on soil, some springs were introduced. In this paper, the boundary conditions are considered as the generalized spring conditions to include the interaction of each span with its adjacent spans (Xu et al., 1999; Bakhtiary et al., 2007):

$$EI\frac{\partial^2 Y(0,t)}{\partial X^2}=K_{\mathrm{rl}}\frac{\partial Y(0,t)}{\partial t}; \tag{2}$$

$$T\frac{\partial Y(0,t)}{\partial X}-EI\frac{\partial^3 Y(0,t)}{\partial X^3}=K_{\mathrm{tl}}Y(0,t); \tag{3}$$

$$EI\frac{\partial^2 Y(L,t)}{\partial X^2}=-K_{\mathrm{r2}}\frac{\partial Y(L,t)}{\partial t}; \tag{4}$$

$$T\frac{\partial Y(L,t)}{\partial x}-EI\frac{\partial^3 Y(L,t)}{\partial X^3}=-K_{\mathrm{t2}}Y(L,t), \tag{5}$$

in which L is the length of the pipe free span; K_{r1} and K_{r2} are the rotatory spring constants for left and right ends of the free span, respectively; K_{t1} and K_{t2} are the translatory spring constants for left and right ends, respectively; and the spring stiffness can be calculated according to the soil stiffness.

We introduce a wake oscillator model for the coupling of the fluctuating drag force and pipeline structure. The fluctuating drag coefficient C'_{D} satisfies the van der Pol equation. A forcing term in the van der Pol equation, which is proportional to the acceleration of the structural motion, is used to represent the effect of structure on the wake. Hence

$$\frac{\partial^2 q}{\partial t^2}+\varepsilon\Omega_{\mathrm{f}}\left(q^2-1\right)\frac{\partial q}{\partial t}+\left(\beta\Omega_{\mathrm{f}}\right)^2 q=\frac{A}{D}\frac{\partial^2 Y}{\partial t^2}, \tag{6}$$

where q is here defined as the local fluctuating drag coefficient of a free spanning pipeline, and $q=2C'_{\mathrm{D}}/C_{\mathrm{D0}}$, in which C_{D0} can be interpreted as the fluctuating drag coefficient of a stationary cylinder. ε and A in Eq. (6) are two independent model parameters to be estimated by considering data on free and forced IL VIV experiments. They must be chosen to provide the best fit to experimental data. $\Omega_{\mathrm{f}}=2\pi StU/D$ is the vortex shedding frequency, St is the Strouhal number.

It is well known that the pure IL VIV consists of two excitation regions: the first one originates from symmetric vortex shedding with a lower reduced velocity of $1.0\leqslant V_{\mathrm{r}}<2.3$, while the second excitation region from alternate vortex shedding with a higher reduced velocity of $2.3\leqslant V_{\mathrm{r}}\leqslant 3.8$. ($V_{\mathrm{r}}$ is the reduced velocity defined by $V_{\mathrm{r}}=2\pi U/(\Omega_{\mathrm{s}}D)$, where Ω_{s} is the natural frequency of a free spanning pipeline) (Sumer and Fredsoe, 1997). In this paper, the same pure IL VIV region is adopted. As discovered by previous researchers, the frequency of IL fluctuating drag force in the first excitation region was approximately three times the Strouhal frequency (Aronsen et al., 2005; Sidarta et al., 2006), and associated with a vortex shedding frequency corresponding to two times the Strouhal frequency in the second excitation region (Currie and Turnbull, 1987). Hence, the parameter β is a multiple of Strouhal frequency, which can be defined as (Xu et al., 2012):

$$\beta=\begin{cases}3, & \text{for } 1.0\leqslant V_{\mathrm{r}}<2.3\\ 2, & \text{for } 2.3\leqslant V_{\mathrm{r}}<3.8\end{cases} \tag{7}$$

The correctness of the prediction results by presenting IL wake oscillator model is determined by empirical parameters ε and A. The empirical wake coefficients may be derived as functions of system parameters defining both the incoming flow and structural properties from a series of experiments. A similar approach in the identification of CF wake oscillator model's empirical coefficients is applied here. The fluctuating drag force q acting on the structure is magnified by an imposed structure motion y (Currie and Turnbull, 1987), and the coupling force scaling A is estimated by analyzing the effects of an imposed motion of the structure on the near wake dynamics (Facchinetti et al., 2004). In this paper, parameter A is determined according to the lock-in bands for synchronization of the vortex shedding with pure IL cylinder vibration (Xu et al., 2012):

$$A=\begin{cases}20, & \text{for } 1.0\leqslant V_{\mathrm{r}}<2.3\\ 8, & \text{for } 2.3\leqslant V_{\mathrm{r}}<2.94\\ 12, & \text{for } 2.94\leqslant V_{\mathrm{r}}<3.8\end{cases} \tag{8}$$

The parameter ε depends on the measured maximum amplitude per cylinder diameter. We propose two curve-fit formulae which are used to describe the experimental measurements of the dimensionless maximum amplitude versus the mass-damping parameter C_{n}(=$4\pi\mu\xi$, where μ is the mass ratio, defined as $M/(\rho D^2)$, and ξ is the structural damping factor) in the first and second IL VIV regions (see Fig. 3). Assuming that the maximum structure displacement amplitude obtained by theoretical analysis is the same as the experimental results, we derive the expressions as follows:

$$\frac{C_{\mathrm{D0}}}{24\pi^2St^2\left(\frac{3C_{\mathrm{n}}}{2\pi}+\gamma\right)}\sqrt{1+\frac{A}{\varepsilon}\frac{C_{\mathrm{D0}}}{16\pi^2St^2\left(\frac{3C_{\mathrm{n}}}{2\pi}+\gamma\right)}}=0.216\mathrm{e}^{-1.866C_{\mathrm{n}}}$$
$$\text{for } 1.0\leqslant V_{\mathrm{r}}<2.3; \tag{9}$$

$$\frac{C_{\mathrm{D0}}}{6\pi^2St^2\left(\frac{C_{\mathrm{n}}}{\pi}+\gamma\right)}\sqrt{1+\frac{A}{\varepsilon}\frac{C_{\mathrm{D0}}}{16\pi^2St^2\left(\frac{C_{\mathrm{n}}}{\pi}+\gamma\right)}}=0.172\mathrm{e}^{-0.949C_{\mathrm{n}}}$$
$$\text{for } 2.3\leqslant V_{\mathrm{r}}<3.8, \tag{10}$$

where γ is the stall parameter, defined as $\gamma=C_{\mathrm{D}}/(2\pi St)$. By combining Eqs. (8), (9) and (10), the empirical parameter ε and A can be obtained. The other parameters C_{D0}, St and C_{D} presented above are given as follows: C_{D0} =0.2 (King, 1977), St=0.17 (Sidarta et al., 2010) and C_{D}=1.2. The values of these parameters are used throughout this paper.

2.2 Dimensionless form

Introduce the following dimensionless variables and parameters

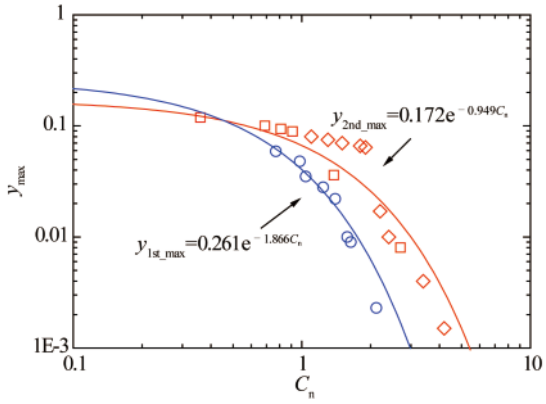

Fig. 3. Dimensionless maximum amplitude of response y_{max} versus mass-damping parameter C_n and the proposed curve-fitting. Experimental data: ○ two-dimensional circular cylinder response amplitude in the water tunnel in the first excitation region (Okajima et al., 2001), □ cantilevered cylinder response amplitude in the water tunnel in the second excitation region (Nakamura et al., 2001), and ◊ two-dimensional circular cylinder response amplitude in the wind tunnel in the second excitation region (Matsuda et al., 2003).

$$y=\frac{Y}{D},x=\frac{X}{L},\tau=\sqrt{\frac{EI}{M}}\frac{t}{L^2},$$

$$m_f=\frac{M_f}{M},v_f=V_fL\sqrt{\frac{M_f}{EI}},c=\frac{C_D\rho DU^2L^2}{\sqrt{MEI}},$$

$$p=\frac{TL^2}{EI},G=\frac{\rho C_{D0}U^2L^4}{4EI},k_{r1}=\frac{K_{r1}}{\sqrt{MEI}},$$

$$k_{r2}=\frac{K_{r2}}{\sqrt{MEI}},k_{t1}=\frac{K_{t1}L^3}{EI},k_{t2}=\frac{K_{t2}L^3}{EI},$$

$$\omega_f=\Omega_fL^2\sqrt{\frac{M}{EI}}\text{ and }\omega_s=\Omega_sL^2\sqrt{\frac{M}{EI}}.$$

Eqs. (1) and (6) can be cast into the dimensionless form

$$\frac{\partial^2y}{\partial\tau^2}+c\frac{\partial y}{\partial\tau}+2\sqrt{m_f}v_f\frac{\partial^2y}{\partial x\partial\tau}+\frac{\partial^4y}{\partial x^4}+\left(v_f^2-p\right)\frac{\partial^2y}{\partial x^2}=Gq; \tag{11}$$

$$\frac{\partial^2q}{\partial\tau^2}+\varepsilon\omega_f\left(q^2-1\right)\frac{\partial q}{\partial\tau}+(\beta\omega_f)^2q=A\frac{\partial^2y}{\partial\tau^2}. \tag{12}$$

The dimensionless general boundary conditions Eqs. (2)–(5) can be written as:

$$\frac{\partial^2y(0,\tau)}{\partial x^2}=k_{r1}\frac{\partial y(0,\tau)}{\partial\tau}; \tag{13}$$

$$p\frac{\partial y(0,\tau)}{\partial\tau}-\frac{\partial^3y(0,\tau)}{\partial x^3}=k_{t1}y(0,\tau); \tag{14}$$

$$\frac{\partial^2y(1,\tau)}{\partial x^2}=-k_{r2}\frac{\partial y(1,\tau)}{\partial\tau}; \tag{15}$$

$$p\frac{\partial y(1,\tau)}{\partial\tau}-\frac{\partial^3y(1,\tau)}{\partial x^3}=-k_{t2}y(1,\tau). \tag{16}$$

3 Modal analysis

The coupled Eqs. (11) and (12) for pure IL VIV of a free spanning pipeline are nonlinear, and then the analytical solutions cannot be obtained. In this section, the nonlinear partial differential equations are reduced to a set of ordinary differential equations by applying the modal analysis method. Assume that the vibration mode of the free span can be described by a superposition of the eigenmodes. Because pure IL VIV of free spanning pipeline is not a stable structure-fluid interaction phenomenon, higher modes cannot be excited (Sidarta et al., 2006; Larsen et al., 2007). In this paper, a second-order modal truncation is adopted:

$$y(x,\tau)=\sum_{i=1}^{2}\phi_i(x)\overline{y}_i(\tau); \tag{17}$$

$$q(x,\tau)=\sum_{i=1}^{2}\phi_i(x)\overline{q}_i(\tau), \tag{18}$$

where

$$\phi_i(x)=c_1\cosh(s_1x)+c_2\sinh(s_1x)+c_3\cos(s_2x)+c_4\sin(s_2x), \tag{19}$$

with s_1 and s_2 are given by

$$s_1=\sqrt{\left[\left(\frac{p-v_f^2}{2}\right)^2+\omega_s^2\right]^{\frac{1}{2}}+\frac{p-v_f^2}{2}}; \tag{20}$$

$$s_2=\sqrt{\left[\left(\frac{p-v_f^2}{2}\right)^2+\omega_s^2\right]^{\frac{1}{2}}-\frac{p-v_f^2}{2}}. \tag{21}$$

c_1, c_2, c_3, and c_4 are constants, and can be obtained from the imposed boundary conditions, and cannot affect the natural frequency. According to the same method used by Xu et al. (1999), the natural frequencies of the free span can be expressed by the following equation:

The effects of internal fluid, axial force and boundary conditions on natural frequencies of the free span will be discussed by Eq. (22) in Section 5.

$$\begin{vmatrix} s_1^2 & -k_{r1}s_1 & -s_2^2 & -k_{r1}s_2 \\ s_1^2\cosh(s_1)+k_{r2}s_1\sinh(s_1) & s_1^2\sinh(s_1)+k_{r2}s_1\cosh(s_1) & -s_2^2\cos(s_2)-k_{r2}s_2\sin(s_2) & -s_2^2\sin(s_2)+k_{r2}s_2\cos(s_2) \\ k_{t1} & s_1^3-ps_1 & k_{t1} & -s_2^3-ps_2 \\ k_{t2}\cosh(s_1)-(s_1^3-ps_1)\sinh(s_1) & k_{t2}\sinh(s_1)-(s_1^3-ps_1)\cosh(s_1) & k_{t2}\cos(s_2)-(s_2^3+ps_2)\sin(s_2) & k_{t2}\sin(s_2)+(s_2^3+ps_2)\cos(s_2) \end{vmatrix}=0. \tag{22}$$

Substituting Eqs. (17) and (18) into Eqs. (11) and (12), multiplying by $\phi_i(x)$ on both sides and integrating from 0 to 1, and utilizing the orthogonality relation of modes, we can obtain four coupled ordinary differential Eqs. (23)–(26) of

$\bar{y}_i$ and $\bar{q}_i$ (we substitute $\bar{y}_i$ and $\bar{q}_i$ for y_i and q_i for writing simplicity)

$$\ddot{y}_1 + c\dot{y}_1 + \vartheta_1 y_1 + \lambda_1(\dot{y}_1, \dot{y}_2) = Gq_1; \tag{23}$$

$$\ddot{y}_2 + c\dot{y}_2 + \vartheta_2 y_2 + \lambda_2(\dot{y}_1, \dot{y}_2) = Gq_2; \tag{24}$$

$$\ddot{q}_1 - \varepsilon\omega_f\dot{q}_1 + (\beta\omega_f)^2 q_1 + \kappa_1(q_1, q_2, \dot{q}_1, \dot{q}_2) = A\ddot{y}_1; \tag{25}$$

$$\ddot{q}_2 - \varepsilon\omega_f\dot{q}_2 + (\beta\omega_f)^2 q_2 + \kappa_2(q_1, q_2, \dot{q}_1, \dot{q}_2) = A\ddot{y}_2, \tag{26}$$

where ϑ_1, ϑ_2, λ_1, λ_2, κ_1, and κ_2 are the coefficients computed from the integrals of the eigenfunctions $\phi_i(x)$ analytically or numerically. They are given as follows:

$$\vartheta_i = \frac{\int_0^1 \left[\frac{\mathrm{d}^4\phi_i(x)}{\mathrm{d}x^4} + (v_f^2 - p)\frac{\mathrm{d}^2\phi_i(x)}{\mathrm{d}x^2}\right] \cdot \phi_i(x)\mathrm{d}x}{\int_0^1 \phi_i(x) \cdot \phi_i(x)\mathrm{d}x}; \tag{27}$$

$$\lambda_i = \frac{2\sqrt{m_f}v_f \int_0^1 \sum_{j=1}^{2} \frac{\mathrm{d}\phi_j(x)}{\mathrm{d}x}\frac{\mathrm{d}y_j(\tau)}{\mathrm{d}\tau} \cdot \phi_i(x)\mathrm{d}x}{\int_0^1 \phi_i(x) \cdot \phi_i(x)\mathrm{d}x}; \tag{28}$$

$$\kappa_i = \frac{\varepsilon\omega_f \int_0^1 \left[\sum_{j=1}^{2} \phi_j(x)q_j(\tau)\right]^2 \sum_{j=1}^{2} \phi_j(x)\frac{\mathrm{d}q_j(\tau)}{\mathrm{d}\tau} \cdot \phi_i(x)\mathrm{d}x}{\int_0^1 \phi_i(x) \cdot \phi_i(x)\mathrm{d}x}. \tag{29}$$

4 Numerical method and verification

The ordinary differential Eqs. (23)–(26) are solved numerically using MATLAB ode45 in this section. A zero IL displacement and velocity are imposed on the initial conditions for the pipeline, and $q_1(0) = q_2(0) = 0.01$ and $\frac{\mathrm{d}q_1}{\mathrm{d}t}(0) = \frac{\mathrm{d}q_2}{\mathrm{d}t}(0) = 0$ are the initial conditions for the fluid variable.

The above prediction model had been applied to calculate the pure IL VIV of a marine pipeline with the pinned-pinned boundary condition in uniform flow, by assuming that k_{r1} and k_{r2} equal zero, and k_{t1} and k_{t2} equal the extreme value, the pinned-pinned boundary condition is obtained. k_{t1} and k_{t2} were approximated by 10^{10} to simply MATLAB programming in this paper, and the numerical results were compared with the experimental data of Huse (2001) and VIVANA results (Larsen et al., 2007). The structural parameters for the pipeline model in Huse's (2001) experiment are given in Table 1, and the experimental set-up is plotted in Fig. 4. According to the comparison of response amplitude which is shown in Fig. 5, we can conclude that the model results agree fairly well with the experimental data, and these results indicate the applicability and usefulness of the above IL wake oscillator model to predict pure IL VIV of free spanning pipelines. Readers can refer to Xu et al. (2012) for more details of the verification.

Table 1 Structural parameters for the pipeline model in Huse's experiment (Huse, 2001)

Parameter (unit)	Value
Length, L (m)	11.413
Outer diameter, D (m)	0.0326
Bending stiffness, EI (N×m^2)	203.0
Axial force, T (N)	67.8
Mass, M (kg/m)	1.147
Damping ratio, ξ	0.4%
Mass ratio, μ=M/(ρD^2)	1.1

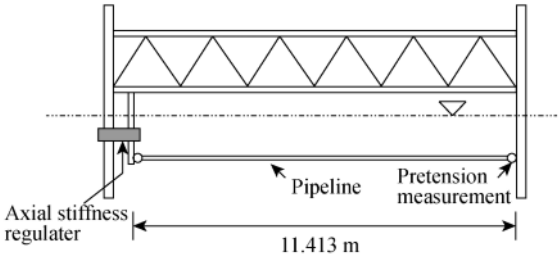

Fig. 4. Experimental set-up in Huse (2001).

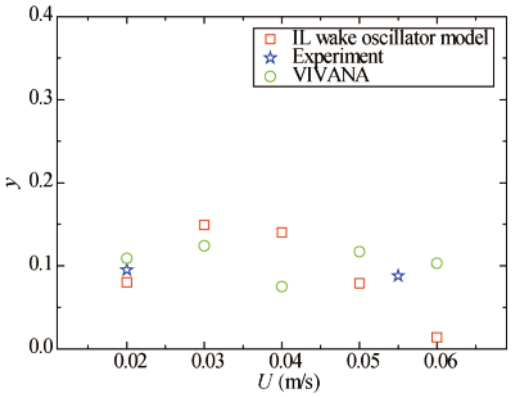

Fig. 5. Response amplitude versus the incoming flow velocity (Xu et al., 2012).

5 Results and discussion

In this section, we investigate the characteristics of pure IL VIV of a free spanning pipeline by utilizing the above IL wake oscillator model, mainly focus on the influence of internal fluid, axial force and boundary conditions on pure IL VIV of the pipeline spans. Three cases studies are carried out; the brief parameters for the simulations are shown in Table 2.

Table 2 Basic input parameters for the simulations of free spanning pipelines

Brief parameters	Case I (Ai et al., 2009)	Case II (Koushan, 2009)	Case III (Larsen et al., 2007)
Outer diameter, D (m)	0.22	0.556	0.4
Length of free span, L (m)	40.0	92.0	50.0
Bending stiffness, EI (N×m^2)	4.02×10^6	2.9×10^8	8.9×10^7
Internal fluid mass, M_f(kg/m)	27.7	30.0	34.0
Structural mass, M_p(kg/m)	63.5	314.9	96.2
Added mass, M_a(kg/m)	39.0	248.9	128.8
Damping ratio, ξ	0.5%	0.3%	0.3%

5.1 Influence of internal fluid

The effects of internal fluid on pure IL VIV of a free spanning pipeline are emphasized in Case I study, the other data used in the calculation of Case I are as follows: the ro-

tatory spring constants k_{r1}=k_{r2}=0.0, and the translatory spring constants k_{t1}=k_{t2}=10^{10}. The pinned-pinned boundary condition is obtained, and in addition, there is no axial force for Case I. The variation of dimensionless internal fluid velocities v_f is 0.0–3.0 with an interval of 1.0. The upper internal fluid velocity does not exceed the critical velocity (v_f=π) which can destabilize the pipe in the absence of drag. The first two frequencies, maximum response amplitude and incoming flow velocity range are calculated. These results are listed in Table 3. It can be observed that the influence of internal fluid on natural frequencies is not obvious when the internal fluid velocity is relatively slow as it is away from the critical value (v_f=π). The natural frequency falls fast near the critical internal fluid velocity. The initial incoming flow velocity, which makes pure IL VIV occur, shifts to a lower value and the incoming flow velocity range becomes narrow with the increasing internal fluid velocity. More details can be seen in Table 3 and Fig. 6 which plot the variation of the first two frequencies Ω_{si} (i=1, 2) with varying internal fluid velocity. Fig. 7 shows the dimensionless response amplitude versus the reduced velocity for varying internal fluid velocity. It can be seen that there are two separate pure IL VIV excitation regions over the reduced velocity ranging from 1.0 to 3.8, and the amplitude of the periodic motion decreases with the increasing internal fluid velocity. This phenomenon becomes more and more remarkable when the internal fluid velocity is closed to the critical velocity. However, the internal fluid velocity in the practical offshore oil and gas engineering is small, and the influence from internal fluid on pure IL VIV of a free spanning pipeline is less significant.

Table 3 Natural frequencies, incoming flow velocity range and response amplitude for the varying internal fluid velocity

Dimensionless internal fluid velocity, v_f	Natural frequencies (Ω_{s1}, Ω_{s2}) (rad/s)	Incoming flow velocity range (m/s)	Response amplitude, y
0.0	(1.0839, 4.3356)	0.0380–0.1442	0.0241
1.0	(1.0275, 4.2803)	0.0358–0.1360	0.0232
2.0	(0.8359, 4.1101)	0.0293–0.1112	0.0210
3.0	(0.3217, 3.8095)	0.0113–0.0428	0.0125

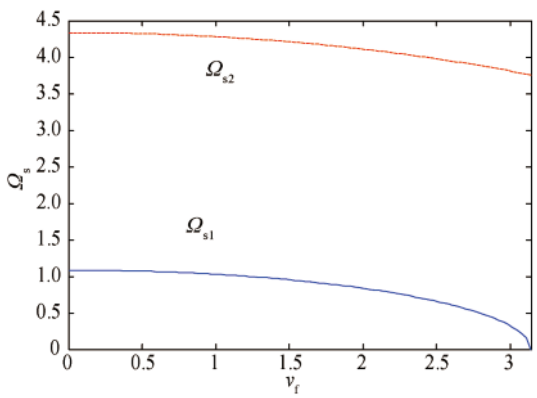

Fig. 6. First two natural frequencies with the increasing internal fluid velocity.

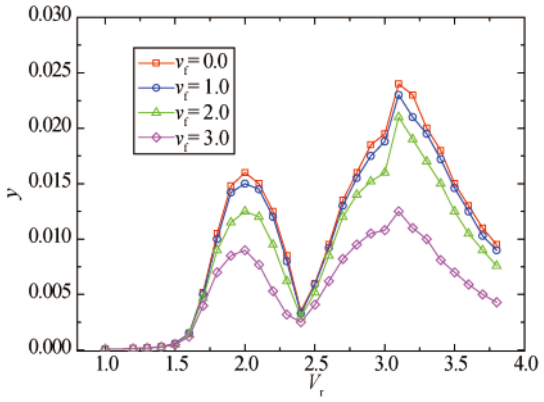

Fig. 7. Response amplitude versus the reduced velocity for the varying internal fluid velocity.

5.2 Influence of axial Force

Axial force in the pipeline will be determined by the internal pressure, temperature gradient and pipe deflection in free spans. We study the influence of the axial force on the pure IL VIV in Case II. The basic input data are listed in Table 2. The other data are: the rotatory spring constants k_{r1}=k_{r2}=10^{10}, and the translatory spring constants k_{t1}=k_{t2}=10^{10}. The boundary is coincided with the fixed-fixed boundary condition, and there is no internal fluid velocity in this case study. The variations of dimensionless axial force p=TL^2/(EI) is from –20.0 to 20.0 with an interval of 10.

Table 4 shows the simulation results of natural frequencies, incoming flow velocity and response amplitude for the varying axial force. It can be found that the natural frequency is seen to have a gradual decrease with the for decreasing axial force; finally, as the axial force approaches the critical buckling load, the frequency approaches zero, and more details are plotted in Fig. 8. The initial incoming flow velocity shifts to a higher value and the incoming flow velocity range becomes wider with the increasing axial force. It seems that the high values of the axial force make pure IL VIV too difficult to occur. From Fig. 9, we found that the dimensionless response amplitude had a gradual increase with the increasing axial force. It was a different phenomenon about the response amplitude with CF VIV. The reason may be that much higher axial force results in a larger initial incoming flow velocity, then the fluctuating drag on the structure turns stronger, and a higher value of the response amplitude is obtained. However, continuous increase of the response amplitude will not happen because of

Table 4 Natural frequencies, incoming flow velocity range and response amplitude for the varying axial force

Dimensionless axial force, p	Natural frequencies (Ω_{s1}, Ω_{s2}) (rad/s)	Incoming flow velocity range (m/s)	Response amplitude, y
–20.0	(1.3084, 4.4296)	0.1158–0.4400	0.0282
–10.0	(1.6026, 4.7731)	0.1418–0.5389	0.0295
0.0	(1.8473, 5.0920)	0.1635–0.6212	0.0311
10.0	(2.0606, 5.3909)	0.1823–0.6929	0.0340
20.0	(2.2519, 5.6729)	0.1993–0.7572	0.0351

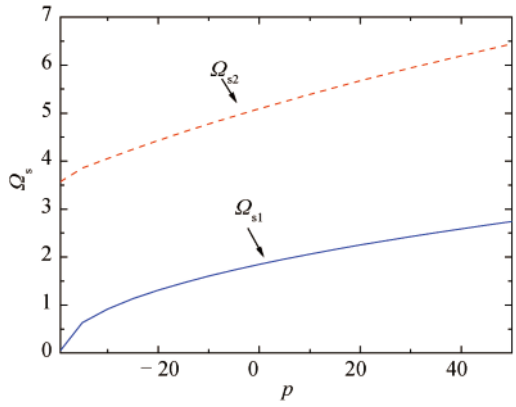

Fig. 8. First two natural frequencies with the increasing axial force.

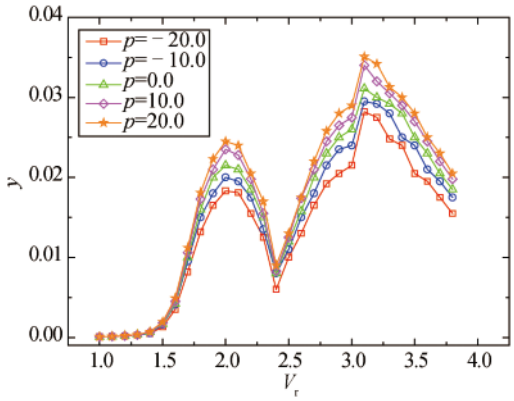

Fig. 9. Response amplitude versus the reduced velocity for the varied axial force.

the self-excitation and self-limitation of pure IL VIV. These results also indicate the complexity of the pure IL VIV issue. More experiments should be carried out further on this subject.

5.3 Influence of boundary conditions

As presented in Section 2, the boundary conditions of the pipe free span are considered as rotatory spring and translatory spring. We analyzed the rotatory spring stiffness k_r and translatory spring stiffness k_t on the pure IL VIV of pipe free span in Case III. The left and right boundary conditions of the pipe free span were supposed to be symmetric. Table 2 lists the basic input data for Case III study. Exceptionally, the axial force T=10 kN and the internal fluid velocity is zero.

First, we consider one sand clay seabed situation and let the value of k_t be equal to 10^5. The value of k_r varies between 1 and 10^4. The results of the natural frequencies, incoming flow velocity and response amplitude for the varying rotatory spring stiffness are listed in Table 5. It is indicated that the natural frequencies have a gradual increase with the increasing rotatory spring stiffness, and the natural frequencies reach constants when the rotatory spring stiffness exceeds the value of 10^4, and more details can be found in Fig. 10. Table 5 also presents that the initial incoming flow velocity becomes higher and the incoming flow velocity range becomes wider with the increasing rotatory spring stiffness. Fig. 11 plots the effects of the rotatory spring stiffness on the response amplitude of the pipe free span. The amplitude of the periodic motion goes up with the increasing rotatory spring stiffness; the values of the maximum response amplitude are listed in Table 5.

Then let k_r=10^2, and the variation of k_t between 10^2 and 10^6 is discussed. Table 5 presents the results of natural frequencies, incoming flow velocity and response amplitude for the varying translatory spring stiffness. The first two natural frequencies and response amplitude versus the reduced velocity for the varying translatory spring stiffness

Table 5 Natural frequencies, incoming flow velocity range and response amplitude for the varying rotatory spring stiffness

Dimensionless rotatory spring stiffness, k_r	Natural frequencies (Ω_{s1}, Ω_{s2}) (rad/s)	Incoming flow velocity range (m/s)	Response amplitude, y
10^0	(2.3852, 9.3218)	0.1518–0.5770	0.0355
10^1	(2.6863, 9.6505)	0.1710–0.6499	0.0377
10^2	(3.9567, 11.5191)	0.2519–0.9572	0.0460
10^3	(5.0343, 13.8524)	0.3205–1.2179	0.0520
10^4	(5.2352, 14.3832)	0.3333–1.2665	0.0531

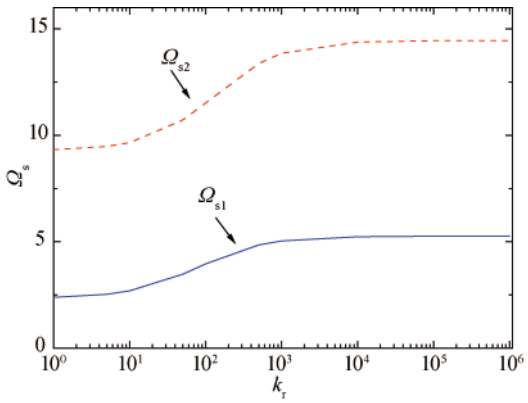

Fig. 10. First two natural frequencies with the increasing rotatory spring stiffness.

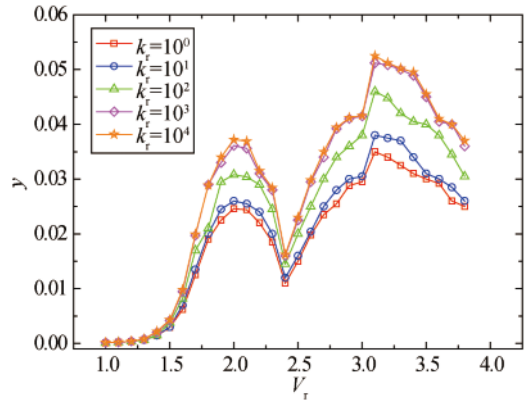

Fig. 11. Response amplitude versus the reduced velocity for the varied rotatory spring stiffness.

are plotted in Fig. 12 and Fig. 13, respectively. It can be found that the translatory spring and rotatory spring own the similar influence on pure IL VIV of a free spanning pipeline. The effects of the translatory spring on the natural frequencies and response amplitude are not obvious at all when the value of the translatory spring stiffness goes beyond 10^4.

Table 6 Natural frequencies, incoming flow velocity range and response amplitude for the varying translatory spring stiffness

Dimensionless translatory spring stiffness, k_t	Natural frequencies (Ω_{s1}, Ω_{s2}) (rad/s)	Incoming flow velocity range (m/s)	Response amplitude, y
10^2	(2.6237, 5.1168)	0.1670–0.6347	0.0371
10^4	(3.9375, 11.3592)	0.2507–0.9525	0.0459
10^6	(3.9586, 11.5352)	0.2520–0.9576	0.0460

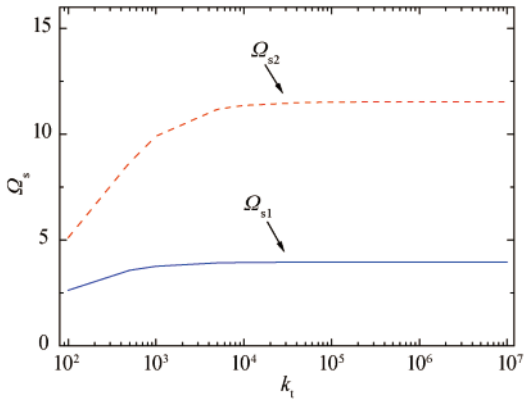

Fig. 12. First two natural frequencies with the increasing translatory spring stiffness.

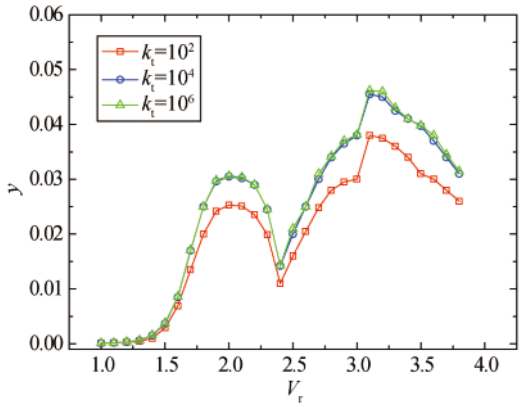

Fig. 13. Response amplitude versus the reduced velocity for the varied translatory spring stiffness.

6 Conclusions

The main contribution of this paper is that the effects of internal fluid and axial force on pure IL VIV of a free spanning pipeline were studied, and three types' boundary conditions were taken into account; a pure IL wake oscillator model was introduced and applied for the investigations.

The simulations demonstrated that internal fluid does not influence the pure IL VIV behaviors obviously; it is a less important factor than other ones, such as boundary conditions and axial force. The effect of internal fluid can be neglected during the pure IL VIV prediction of the pipeline spans. The comparison results of three different boundary conditions showed that the frequency, response amplitude and incoming flow velocity range are strongly dependent on boundary condition. The pure IL VIV behaviors are considerably different under various boundary conditions. Another important finding is that the axial force makes the emergence of some interesting phenomena on the pure IL VIV of the free spanning pipeline, such that the response amplitude becomes larger when the axial force increases.

Moreover, a series of pure IL VIV experimental measurements of a free spanning pipeline conveying fluid are needed to find more interesting IL VIV phenomena, as well as benchmarking against the future predicted numerical outcomes by IL wake oscillator model.

References

Ai, S.M., Sun, L.P. and Ma, G., 2009. The effect of soil non-linearity on VIV response of a free spanning pipeline, *Proceedings of the 28th International Conference on Offshore Mechanics and Arctic Engineering*, Hawaii, USA, OMAE2009–79063.

Aronsen, K.H., Larsen, M.C. and Mørk, K., 2005. Hydrodynamic coefficients from in-line VIV experiments, *Proceedings of the 24th International Conference on Offshore Mechanics and Arctic Engineering*, Halkidiki, Greece, OMAE2005–67393.

Blevins, R.D., 1990. *Flow Induced Vibrations*, Van Nostrand Reinhold, New York.

Choi, H.S., 2001. Free spanning analysis of offshore pipelines, *Ocean Eng.*, 28(10), 1325–1338.

Currie, I.G. and Turnbull, D.H., 1987. Streamwise oscillations of cylinders near the critical Reynolds number, *J. Fluid. Struct.*, 1(2), 185–196.

Dai, H.L., Wang, L. and Qian, Q.N., 2013. Vortex-induced vibrations of pipes conveying fluid in the subcritical and supercritical regimes, *J. Fluid. Struct.*, 39, 322–334.

Facchinetti, M.L., De Langre, E. and Biolley, F., 2004. Coupling of structure and wake oscillators in vortex-induced vibrations, *J. Fluid. Struct.*, 19(2), 123–140.

Furnes, G.K. and Berntsen, J., 2003. On the response of a free span pipeline subjected to ocean currents, *Ocean Eng.*, 30(12), 1553–1577.

Fyrileiv, O., 2010. Effect of internal pressure on free spanning pipelines, *Proceedings of the 8th International Pipeline Conference*, Alberta, Canada, IPC2010–31622.

Gabbai, R.D. and Benaroya, H., 2005. An overview of modeling and experiments of vortex-induced vibration of circular cylinders, *J. Sound Vib.*, 282(3), 575–616.

Huang, Y.M., Liu, Y.S., Li, B.H., Li, Y.J. and Yue, Z.F., 2010. Natural frequency analysis of fluid conveying pipeline with different boundary conditions, *Nucl. Eng. Des.*, 240(3), 461–467.

Huse, E., 2001. *Ormen Lange 3D Model Tests*, MARINTEK Report MT51-F01.040, Trondheim, Norway.

King, R., 1977. A review of vortex shedding research and its application, *Ocean Eng.*, 4(3), 141–171.

Koushan, K., 2009. *Vortex Induced Vibrations of Free Span Pipelines*, Ph. D. Thesis, Norwegian University of Science and Technology (NTNU), Norway.

Larsen, C.M., Yttervik, R. and Aronsen, K., 2007. Calculation of in-line vortex induced vibrations of free spanning pipelines, *Proceedings of the 26th International Conference on Offshore Mechanics and Arctic Engineering*, California, USA, OMAE2007–29533.

Lee, L., Allen, D., Pontaza, J.P., Kopp, F. and Jhingran, V., 2009. In-line motion of subsea pipeline span models experiencing vortex-shedding, *Proceedings of the 28th International Conference on Offshore Mechanics and Arctic Engineering*, Hawaii, USA, OMAE2009–79084.

Lou, M., Ding, J., Guo, H.Y. and Dong, X.L., 2005. Effect of internal flow on Vortex-induced Vibration of submarine free spanning pipeline, *China Ocean Eng*., 19(1), 147–154.

Matsuda, K., Uejima, H. and Sugimoto, T., 2003. Wind tunnel tests on in-line oscillation of a two-dimensional circular cylinder, *Journal of Wind Engineering and Industrial Aerodynamics*, 91(1), 83–90.

Nakamura, A., Okajima, A. and Kosugi, T., 2001. Experiments on flow-induced in-line oscillation of a circular cylinder in a water tunnel (2nd report, influence of the aspect ratio of a cantilevered circular cylinder), *JSME International Journal Ser. B*, 44(4), 705–711.

Okajima, A., Kosugi, T. and Nakamura, A., 2001. Experiments on flow-induced in-line oscillation of a circular cylinder in a water tunnel (1st report, the difference of the response characteristics when a cylinder is elastically supported at both ends and cantilevered), *JSME International Journal Ser. B*, 44(4), 695–704.

Sarpkaya, T., 2004. A critical review of the intrinsic nature of vortex-induced vibrations, *J. Fluid. Struct*., 19, 389–447.

Sidarta, D. E., Finn, L. D. and Maher, J., 2010. Time domain FEA for riser VIV analysis, *Proceedings of the 29th International Conference on Offshore Mechanics and Arctic Engineering*, Shanghai, China, OMAE2010–20688.

Sidarta, D.E., Lambrakos, K.F., Thompson, H.M. and Burke, R.W., 2006. A methodology for In-Line VIV analysis of risers in sheared currents, *Proceedings of the 25th International Conference on Offshore Mechanics and Arctic Engineering*, Hamburg, Germany, OMAE2006–92431.

Sumer, B.M. and Fredsoe, J., 1997. *Hydrodynamics Around Cylindrical Structures*, World Scientific Publishing Company.

Vedeld, K., Sollund, H. and Hellesland, J., 2013. Free vibrations of free spanning offshore pipelines, *Eng. Struct*., 56, 68–82.

Williamson, C.H.K. and Govardhan, R., 2008. A brief review of recent results in vortex-induced vibrations, *Journal of Wind Engineering and Industrial Aerodynamics*, 96(6-7), 713–735.

Xu, T., Lauridsen, B. and Bai, Y., 1999. Wave-induced fatigue of multi-span pipelines, *Mar. Struct*., 12(2), 83–106.

Xu, W.H., Gao, X.F. and Du, J., 2012. The prediction on in-line vortex-induced vibration of slender marine structures, *Acta Mechanica Sinica*, 28(5), 1303–1308.

Yaghoobi, M., Mazaheri, S. and Jabbari, E., 2012. Determining natural frequency of free spanning offshore pipelines by considering the seabed soil characteristics, *Journal of the Persian Gulf* (*Marine Science*), 3(8), 25–34.

Yeganeh Bakhtiary, A., Ghaheri, A. and Valipour, R., 2007. Analysis of offshore pipeline allowable free span length, *Int. J. Civ. Eng*., 5(1), 84–91.